

## Uniaxial Tensile Test Simulation with Bonded Particles Model

Abdelkader Ammeri, Mondher Neifar

(College of Engineering in Al-Qunfudah/ Umm Al-Qura University, KSA)

---

**Abstract:** The simulation of the direct tensile test by the Discrete Elements Method (DEM) has been done. The generation of homogeneous and isotropic test tubes was made by the numerical process of "radius expansion and friction decrease." The effect of the micro-mechanical parameters on the tensile strength has also been studied. Normal and tangential adhesion and stiffness are the parameters that affect the tensile behavior, while the friction coefficient was ineffective.

**Keywords:** tensile test – numerical simulation - Discrete element method

---

Date of Submission: 10-01-2020

Date of Acceptance: 27-01-2020

---

### I. Introduction

The determination of the tensile strength has been the subject of several researches. Indeed, given the difficulty of performing direct-tensile test on a significant number of materials, several authors have investigated indirect tensile tests [1], [2][3]. The numerical simulation of the direct tensile test has also been the subject of several researches [4]. In particular, there has been intense use in recent years of the DEM to simulate tensile tests [4][5][6]

The model was developed using the commercial code "Particle Flow Code in 2 Dimensions" PFC2D. The model is developed in programs associated with the PFC2D code, using the Fish language.

As with any numerical model, a set of parameters is to be introduced to simulate the problem studied. The parameters can be categorized into two categories: the first grouping purely numerical parameters, conditioning convergence and ensuring the optimality of the solutions, while the second category groups the physical parameters necessary to reconcile the numerical model to the real simulated problem. In order to make good use of the numerical model, both parameter categories must be carefully chosen.

A parametric study of the model has been developed. It is assumed, as is the case in the laboratory, the numerical simulation of the direct tensile test poses more difficulties than all other types of indirect tensile tests. As a result, the parametric study is chosen to analyze the sensitivity of the model on the basis of the uniaxial tensile test.

The first part presents the numerical technique adapted to carry out the tensile test. The second part examines the minimum conditions to be met to ensure the convergence of the model. The third part is dedicated to the micro-macro transition in order to analyze the tensile behavior of a material and the role that micro-mechanical parameters can play.

### II. Model chart

The development of models representing a material that is not perfectly granular (in the sense that the grains that make it up are not of a unique and known form and that the physical interactions between them are also not well known) by a set of particles glued to each other to their contacts, requires an extensive set of support algorithms that guarantee the different stages the analogy between the real problem and the simulated problem. There are four processes in the phase-in of numerical simulation:

- 1- Creating rectangular test tubes of fixed geometry with a given granulometric distribution.
- 2- Attribution of micro-mechanical characteristics and physical properties corresponding to the soil sample studied.
- 3- Performing the tensile test.
- 4- Recording the response of the test tube in tensile during the computational cycles.

Direct tensile test

we present the influence of the different parameters that determine the optimality of convergence, the reproducibility of the test and the consistency of the results.

#### Preparing test tubes

As is the case in the laboratory, in order to perform the uni-axial tensile test, the test tubes must be homogeneous and initially isotropic. For this, the procedure of Expansion of the Radius and Decrease of The Friction (ERDF) [2] was used. It is recalled, in this regard, that the entities used in 3D simulations are spherical

particles and rigid plan walls. These features are reduced to disks and linear walls in the 2D case. The discs represent the particles, while the walls are used to apply the boundary conditions.

In order to create rectangular test tubes for tensile testing, the geometry of the test tube and its granulometry must be defined. It should be remembered here that the defined granulometry may correspond to the actual granulometry of the soil in the case of sands, for example, or in cases where one is interested in phenomena involving the size of particles. However, in the study conducted during this research work, introducing actual granulometry leads to huge computational times due to the large number of particles required for simulation. Therefore, the granulometry introduced in this study represents only a particular pattern of discretization of the field of study.

The granulometry used is defined by the data of the different granular classes that make up the material as well as by their respective volume fractions. A granular class is defined by a "uniform" distribution in diameter of particles between a minimum diameter and a maximum diameter.

The figure 1 shows an example of a G1 granulometry characterized by the data in the table 1

**Table 1:** material granulometry

G1	Granular class	Diameter min (mm)	Diameter Max (mm)	Volume fraction (%)
	Class 1	0,22	0,42	40
	Class 2	0,08	0,22	60

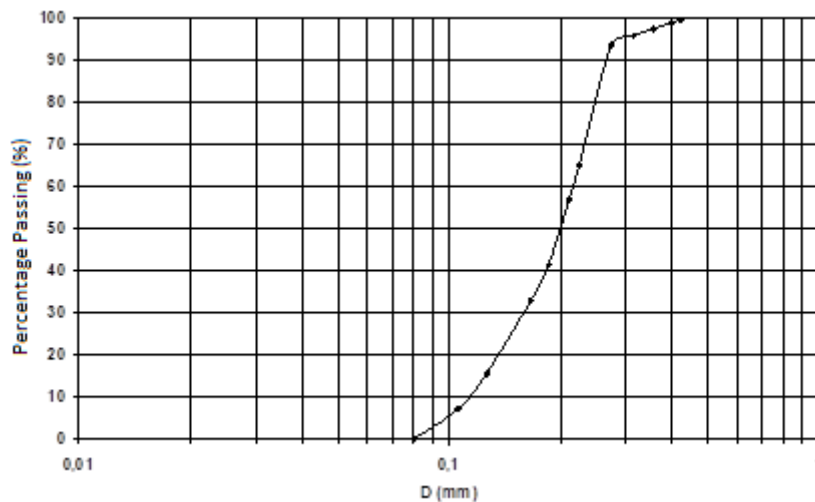


**Figure 1:** Granulometric curve of the material

For a fixed granulometry (Figure 1), a rectangular test tube can be created by the ERDF procedure while fixing the porosity or voids index as well as the state of the initial confinement (figure 2).

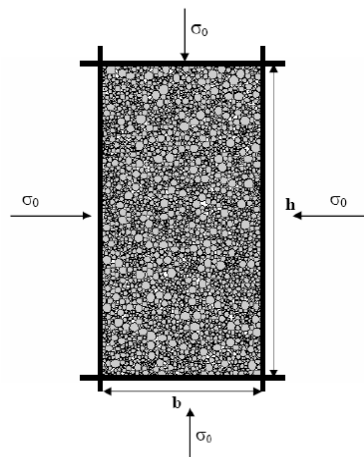


**Figure 2:** Compacting the test tube for the uni-axial tensile test

The range of porosity that can be achieved is between a maximum porosity, beyond which the stability of the assembly can no longer be ensured by the micromechanical parameters implemented, and a minimum porosity corresponding to the densest geometric assembly that can be obtained without friction under a given stress. The convergence of the implementation procedure is therefore not systematically assured when the desired porosities are for a given confinement stress outside the permissible range. Therefore, a comparison of the desired void index  $e_0$  and confinement stress  $\sigma_0$  with the void index  $e_1$  and the confinement stress  $\sigma_1$  obtained is necessary to judge the convergence of the numerical procedure.

This is highlighted on the figure 3 that shows the variation, based on the desired initial void index  $e_0$ , of the void index obtained  $e_1$  as well as the ratio  $\sigma_1/\sigma_0$  for a given initial confinement stress  $\sigma_0$  and a fixed granulometry.

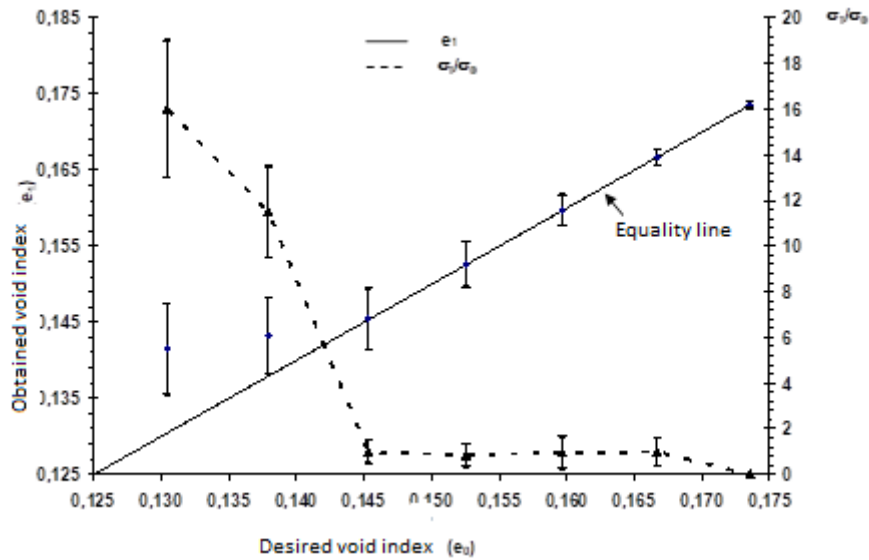


Figure 3: Convergence of the ERDF procedure

Each point of the curves of the figure 3 represents the average of 10 tests, and the length of the segments corresponds to the standard deviation of the values obtained.

According to the figure 3, the ERDF procedure is indeed converging as long as the value of the void index is between the two limits  $e_{min}$  and  $e_{max}$  that depend on the selected granulometry (0.145 and 0.167 respectively). Indeed, for index values of voids below  $e_{min}$  (0.145 for the case treated in the figure 3) the confinement stress necessary to obtain the desired porosity should take important values that allow to artificially increase the interpenetration of particles (or the rearrangement of particles) and thus reduce porosity. For porosity values greater than  $e_{max}$  (0.167) we obtain a very loose set whose insufficient number of contacts does not allow the resulting confinement stress to be obtained. Moreover, the figure 4 shows the evolution of the number of coordination during the ERDF procedure for two porosity values. For a porosity of 0.167 the assembly is stable and compact ( $C_n \cong 3$ ), while for a porosity of 0.21 the assembly is very loose with a number of contacts between the discs insufficient to ensure the proper implementation of the sample ( $C_n \cong 1$ ) (Figure 4).

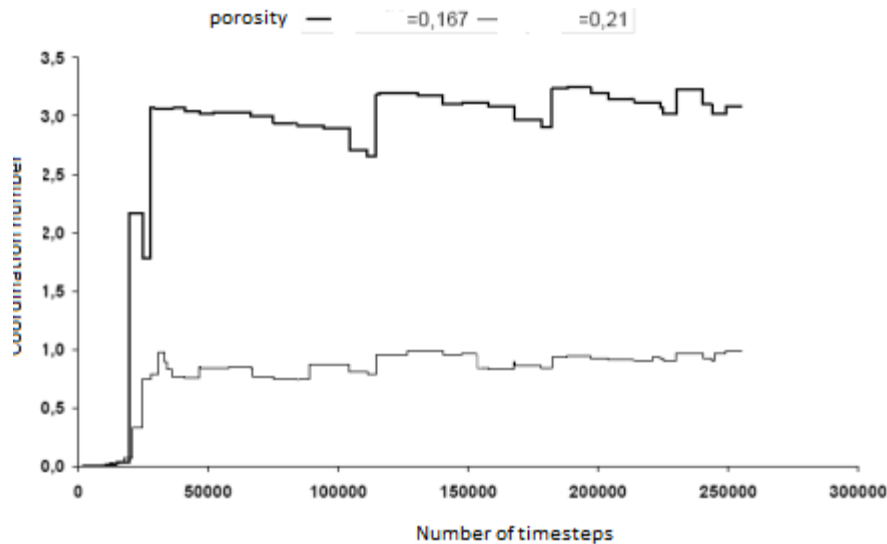


Figure 4: Changes in coordination number during the ERDF procedure

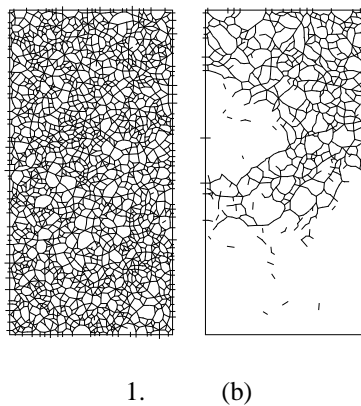


Figure 5: Contact chain of a sample for two porosities (a) 0.167 (b) 0.210.1

Note that for the optimal use of the ERDF procedure for the creation of a homogeneous and isotropic compact assembly, it is necessary to choose the computational time step. The latter must be small enough to be able to admit the hypothesis: "for a short time, disturbances cannot spread further than to the immediate vicinity of a particle". This can be calculated automatically from the rigidities of the contacts and the masses of the particles. The calculation conducted with a given step of time provides a real dynamic response of the assembly during the expansion of the radius. However, during the creation phase of grain assembly, we are only interested in the final quasi-static solution (where the acceleration of all particles becomes zero) we can therefore impose a unit time step which reduces the number of cycles necessary to achieve the final near-static solution. On the other hand, the calculation conducted with an equal imposed time step to the unit does not provide the true intermediate dynamic response.

**Performing the tensile test**

The experimental difficulties presented by the tensile test still remain numerically in the case of discrete elements. Indeed, wall-particle contacts are modeled by springs that work only in compression. Therefore, we cannot pull the particles through the walls. Thus, the test tubes were pulled by digitally creating tensile bits positioned at both ends of the test tube. These tensile bits are made up of particles with very resistant contacts compared to the contacts between the discs representing the particles of the tested material (Figure 6). The two pull bits are similar and are each composed of two parts:

-**Part 1:** Consisting of a material with contact between particles four times more resistant (having contact adhesives of values equal to four times the adhesion in the material) than the contacts of particles representing the material tested and on which conditions in force or on the move are imposed to exert tensile effort.

-**Part 2:** Consisting of a material with contacts twice as strong as the contacts of particles representing the tested material and which constitutes a transition zone between the tensile zones and the sample tested.

The test was conducted on controlled displacement, imposing a velocity on the tensile bit particles (parts 1). Tensile efforts are then transmitted through adhesion between the particles of the bits and those of the material. It is important to ensure that the failure does not occur at the contact bit-material which is potentially possible due to inertial and dynamic effects resulting from excessive particle movement speeds. Tensile force is the sum of unbalanced efforts acting on particles in the upper and low parts (parts 1).

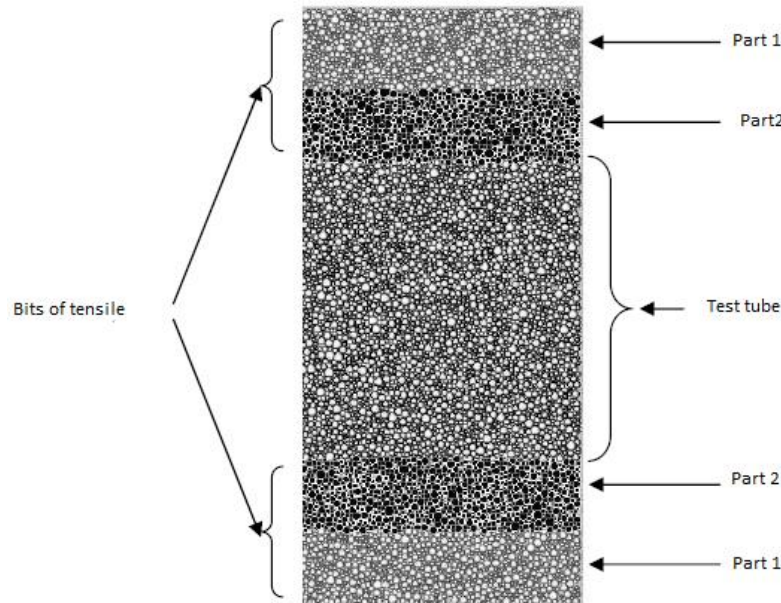


Figure 6: Model of the uni-axial tensile test

### Material properties

In addition to the difficulty of preparing a compact, homogeneous and isotropic digital assembly, it is still necessary to be able to simulate a material whose behavior is similar to that of a real material. For codes based on continuous media assumptions, input properties (such as stiffness and failure criterion) can be deduced directly from measurements taken from laboratory tests. For discrete element codes such as PFC2D the macroscopic behavior of the material is deduced from the interactions of microscopic components.

The calibration procedure of the model must be developed according to the physical problem studied, because there is no complete theory (in the sense of the integration of all forms and distribution of heterogeneities) that allows to predict macroscopic behavior from microscopic properties. It is recalled, while the characteristics of the material are micro-mechanical type defined in the contact between particles. One may then wonder what is the most appropriate micro-mechanical contact law to simulate the macro-mechanical behavior of the material tested and what set of micro-mechanical parameters to choose?

To answer these questions, two approaches are generally adapted by users of DEM, the first approach consists of a micro-micro calibration while the second considers a micro-macro calibration.

For micro-micro calibration, grain-scale measurements are required to determine the parameters of the rheological model. Tests carried out on a grain of the material are digitally reproduced on a single grain, and the contact law obtained is generalized for the entire material. This calibration technique requires sophisticated equipment with the precision of grain-scale measurements. It is generally suitable for model granular materials with regular-shaped grains.

In contrast to this method, micro-macro calibration allows the material to be restored to a global behaviour without seeking to reproduce in a fine way the geometry of the particles, their number and the actual laws of contact of the material.

It should be remembered that a law of contact between two particles is necessarily defined by the association of a law of rigidity with a Coulomb-type slip law. An optional membership law may also be associated with the other two laws. The law of rigidity corresponds to the elastic part of the behaviour, the sliding law serves to limit the shear forces according to the normal forces acting at the contact level, while the adhesion law serves to limit normal forces and tangential behaviour acting at the level of contact and describing post-elastic behaviour. When one of the two normal or tangential adhesions is reached, the cohesive bond is completely broken (simultaneous loss of normal and tangential adhesions) (ITASCA, 2004).

An analysis of the experimental tests carried out on the silty soil studied, can help us in the choice of contact laws to use to describe its behavior. The figure 7 presents some experimental results of simple compression, split tensile, bending and Mohr circles of corresponding stresses.

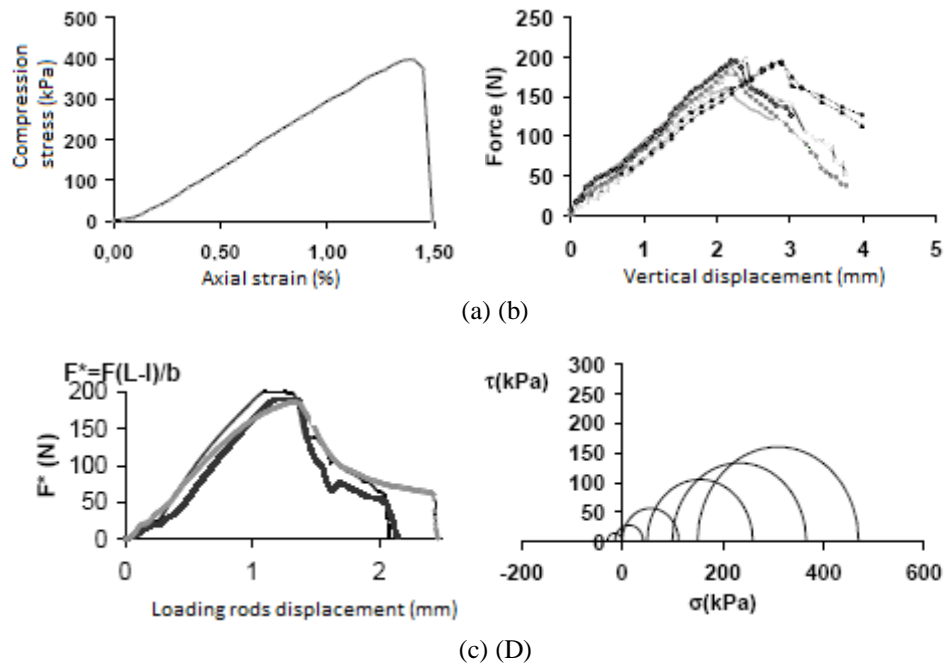


**Figure 7:** Curves "stress-strain": (a) simple compression (b) Split (c) bending four points and Mohr circles of stresses (d)

The three curves (a), (b) and (c) of the figure 7 are in the first part almost linear, which excludes the use of a law of nonlinear rigidity (at least for the silt subject of this study). Therefore, a law of linear stiffness will be retained, this law is defined by the two stiffness, normal and tangential respectively  $K_n$  and  $K_s$ .

The part (d) of the figure 7 shows a rubbing material whose tensile strength is not zero (if one simply extrapolates the envelope of Mohr Coulomb until the interval of normal negative stresses). The validity of the Coulomb-type friction law, defined by a coefficient, is accepted at the contact between two grains  $\mu$ .

Through these two laws, the behavior of purely rubbing materials, such as sands, is usually approached. On the other hand, for coherent materials, there should be a law to integrate particle adhesion. Therefore, to simulate the effect of silt cohesion, a law of adherence to the law of rigidity and the law of slippage is added to the model. This integrates the material's tensile behavior. The adhesion is at the level of contact since it is according to the curves (a) (b) and (c) of the figure 7 of a fragile elastic behavior. This law is completely defined by the two values of normal strength  $C_n$  and tangential  $C_s$  of contact.

Finally, the contact law chosen to simulate the behavior of the silt is defined by a set of micro-mechanical parameters defined at the contact level:

$$P_{micro} = \{K_n, K_s, \mu, C_n, C_s\}$$

Later in this chapter, when the parameter is not subject to a variation, the following values are adopted:

$$K_n/K_s=1; K_n=7,000,000 \text{ N/m}$$

$$C_n/C_s=1; C_n=320,000 \text{ N/m}$$

$$\mu=0.2;$$

$$\gamma= 20 \text{ kN/m}^3$$

Remember that the normal and tangential cohesive boundary forces between the grains are defined by and with and with the rays of the particles in contact. This makes the model independent of the size of soil particles' discretization to the  $C_n$  and  $C_s$  parameters.

$$C_n \cdot \min(ray_1, ray_2)$$

$$C_s \cdot \min(ray_1, ray_2)$$

### III. Optimizing the tensile test

The simulation of a uniaxial tensile test must meet the convergence criteria of the numerical model in order for the results to be usable. In addition to the laws of contact and the parameters that define them, the assembly of particles (geometric shape, number and porosity) and the speed of deformation must be optimized to ensure the convergence of the model towards the right solution.

#### Discretization of the domain

The discretization of the domain corresponds to the definition of granulometry as well as the porosity of the assembly. For a given geometry, and for a granulometry corresponding to grains of small diameters, the number of particles is important. Certainly, managing a high number of particles is like setting aside a large memory space (RAM), and a high computational time is required for numerical simulation. The optimization of the discretization is then essential to make the simulation in a "reasonable" time without losing precision on the solution sought. In this objective several tensile tests were carried out at different numbers of particles.

The figure 8 shows that the stress-deformation curve, corresponding to the direct tensile test, depends on the number of particles used for the simulation. From 2000 particles (about 30 particles on the width of the sample tested) it is possible to ensure the convergence of the problem posed and the dispersion on the results, in terms of strength to tensile, begins to become weak. It should be noted that, in the range of particles tested, the tensile module is virtually insensitive to the number of particles used. However, the figure shows the dependence of strength to the apparent tensile of the number of particles used in the simulation.

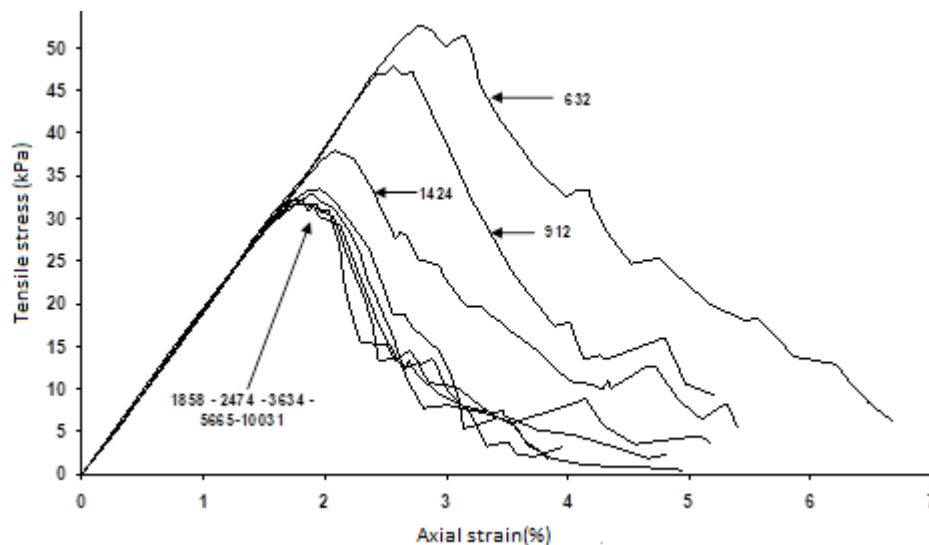


Figure 8: Result of direct tensile test at different numbers of particles

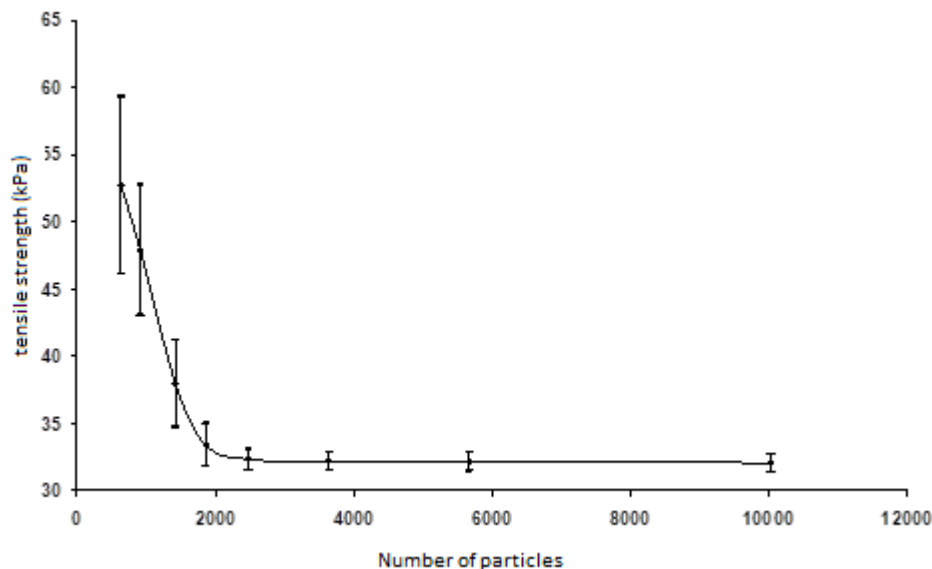


Figure 9: Apparent tensile strength based on the number of particles

The figure 10 represents a histogram of the contact chains before and during the test at the time when the maximum tensile strength is reached (peak value). It is obvious that depending on the loading path, a privileged orientation of the contacts is organized.

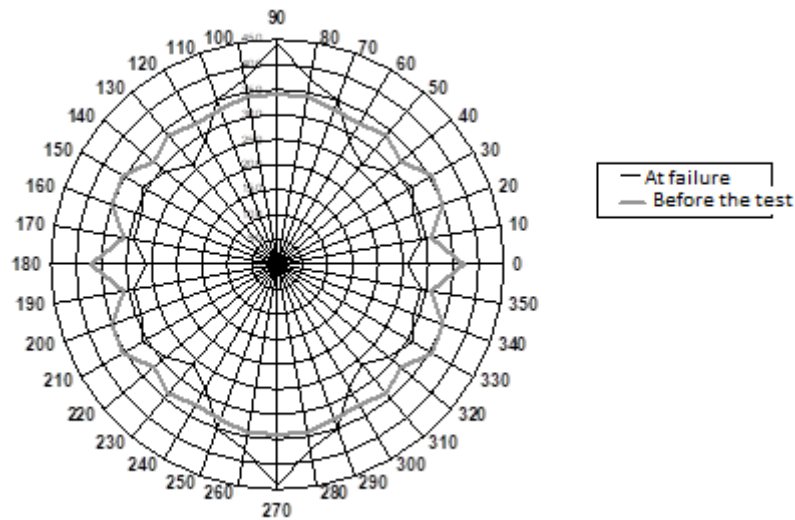


Figure 10: Histogram of contact chains before the test and at the peak

In addition to the number of particles used in a simulation, the shape of the particles can also influence the response of the material. While the particles used in PFC2D have an idealized disk shape, other forms can be created by associating particles with one another. Since then, elongated particles have been created by the association of two discs of different diameters (Figure 11). The association is ensured by a rigid parallel membership. The figure 12 shows that the shape of the base particle has a significant influence on the macroscopic behavior of the material and in particular on the elastic behavior by the fact that the rigid bond between the grains limits at this point any interpenetration or overlap that would have occurred without a rigid link. On the other hand, the peak constraint is little affected by the shape effect in the range tested.



Figure 11: Elongated particles obtained by disk assembly

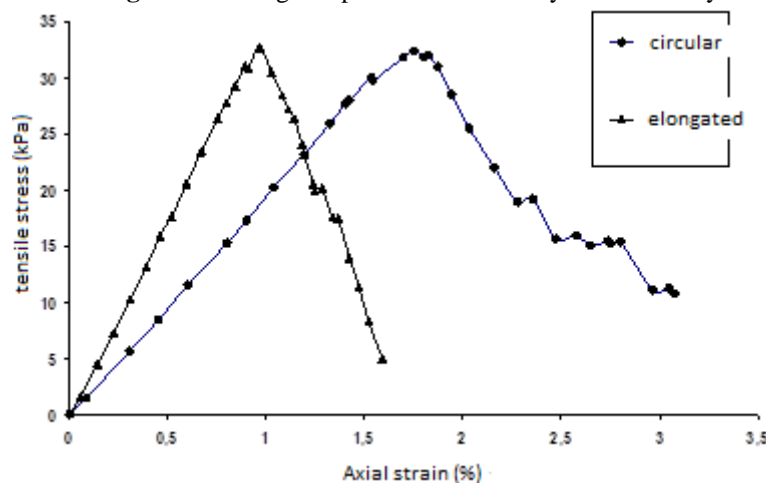
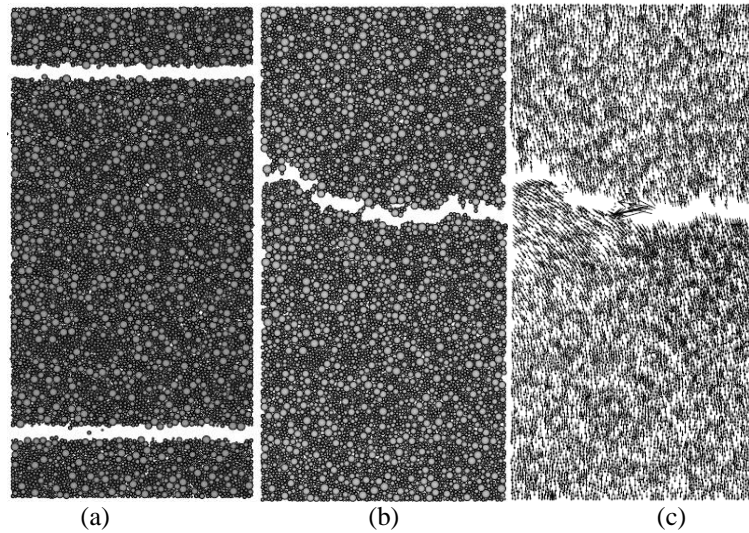


Figure 12: Stress – strain curves during tensile test for circular particles and elongated particles

### Optimizing the speed of the tensile test

During the solid-axial tensile test, the deformation speed must be low enough to keep the sample in a near-static state of equilibrium throughout the test. It is important to ensure that the dynamic and inertial effects are negligible to avoid unfounded and premature ruptures of contact that may result from the propagation of the

waves within the sample. Controlling near-staticity, in other words without having the effects of the acceleration introduced by the numerical scheme, would allow the obtaining of an adequate value of the deformation speed. This control is carried out according to several criteria verified simultaneously. First of all the break mode can be useful to rule out speeds that may be considered too high. The figure 13 shows the rupture of a sample for two different speeds, the first velocity is exaggerated and leads to a sudden break at the bits due to the force of inertia too large. The second rupture is kinematically permissible, but the validity of the chosen speed field must be reinforced by more precise quantitative criteria.



**Figure 13:** (a) Ineligible failure (too high speed); (b) Eligible failure (low speed); (c) velocity field

This has been the adoption of a second criterion for judging the optimality of the deformation velocity, which consists of stopping the loading during the elastic phase and then stabilizing the sample. Once the load is stopped, the tensile stress developed within the sample should, in principle, remain constant if the system is in a quasi-static state. However, the figure 14 shows that the tensile constraint continues, for the chosen deformation speed range, to increase. This is due to an excess of energy that has turned in part into kinetic energy diffused within the particle assembly.

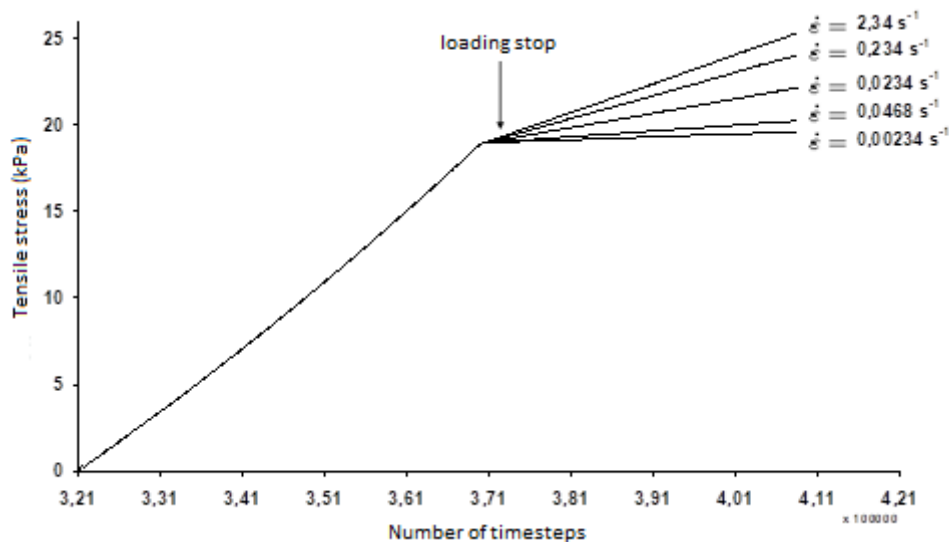


**Figure 14:** Search for optimal speed by stopping loading

A third criterion for judging the optimality of the deformation speed is to control the overall balance of the system during the tensile test, which in fact results in the verification of Newton's second law at the level of each contact. Indeed, each particle must pass during the test through a succession of static equilibrium states. This balance is ensured by a zero value of the resulting forces exerted on each particle. Thus, to control near-staticity, the result of the forces is calculated for each particle during each step of time. The amplitude of the

force exceeding the equilibrium corresponds to what is called "unbalanced force. For a particle assembly, near-staticity is judged by the average value of the amplitude of the resulting unbalanced forces related to the maximum value of the amplitude of the contact forces. Speed is considered permissible when the ratio tends to zero.

The figure 15 shows the ratio of the average value of the magnitude of the resulting unbalanced forces to the maximum contact forces (called the standardized average of unbalanced forces) over time. For the deformation speed of  $2.34 \text{ s}^{-1}$ , it exceeds 0.25 while it reaches only 0.003 for the deformation speed of  $0.024 \text{ s}^{-1}$ .

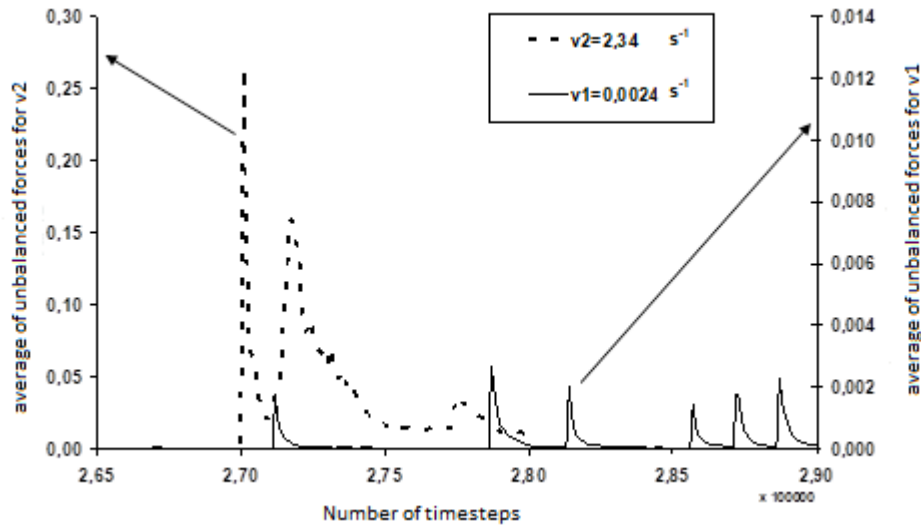


Figure 15: Standardized average of unbalanced forces for two different speeds

Finally a low speed value checking both the three criteria mentioned above can be adopted to carry out the uni-axial tensile test, and in this case one can obtain behavior that is supposed to be independent of the loading speed. However, an improvement in the application of speed can still be made to erase as much as possible its effect on behavior. When the bits are moved at a given speed, a speed gradient occurs and a deformation velocity waves propagate through the sample. As the sample is still in elastic phase, dissipation of excess energy can only take place through non-viscous damping. Therefore, a gradual increase in velocity according to the equation  $(V(t))$  from zero to the chosen optimal value (Figure 16) greatly reduces the speed gradient.

$$V(t) = V_f \left( 1 - e^{\left(-n \frac{t-t_0}{t_{95}}\right)} \right)$$

With

$V_f$ : The deformation speed to be imposed

$t_0$ : The initial time

$t_{95}$ : The time at which  $V(t)$  achieve 95% of  $V_f$

$n$ : Positive number that determines the speed of reaching  $V_f$ . For the curves of the figures 15 and 16  $n$  is equal

3.

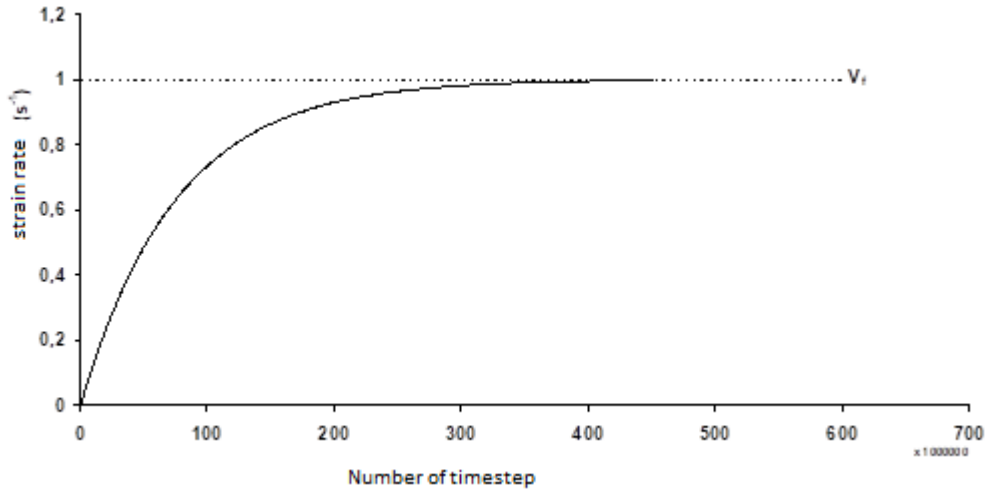


**Figure 16:** Speed progressivity according to time step

Standardized averages of unbalanced forces were plotted (figure 17) for the same deformation speed of  $0.0024 \text{ s}^{-1}$ , but with constant and progressive speeds. It is noted that the gradual application significantly decreases the unbalanced forces in the system and allows for better convergence. It should also be noted that the gradual application of speed requires a significant amount of computational time because the speed must be updated with each cycle.

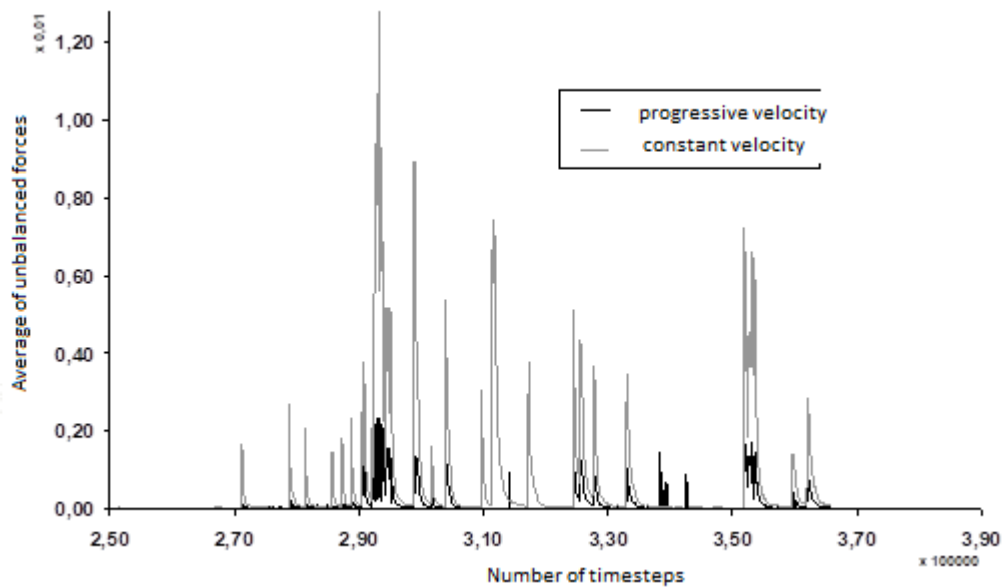


**Figure 17:** Standardized average of unbalanced forces for progressive and constant speed

Finally, macroscopically the applied deformation speed only affects the value of the peak tensile stress (Figure 18), while the rigidity module remains insensitive to the value of the speed.

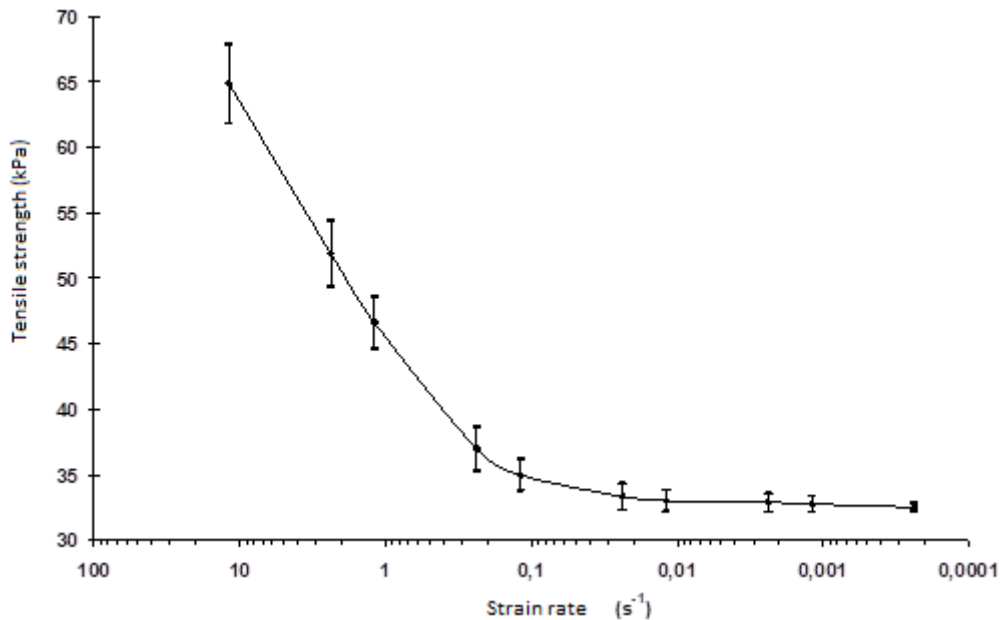


**Figure 18:** Strength to "apparent" tensile based on deformation speed

#### IV. Influence of micro- model properties on tensile behavior

Having chosen a contact law with linear rigidities, Coulomb-type slippage and point contact adhesion, all the dimensionless or representative parameters that can influence tensile behavior are:

$$P_{micro} = \left\{ Cn, Kn, \frac{Cn}{Cs}, \frac{Kn}{Ks}, \mu \right\}$$

During the tensile test the contact points will be used, following normal or tangential movements between particles, normal stresses (usually tensile) and tangential stresses. The rupture of the sample will therefore occur by breaking the contacts in tensile or shear depending on whether the cohesive tensile or shear criterion will be predominant, hence the obvious influence of the Cn and Cs parameters on the sample rupture constraint. In addition, for the same kinematic splendor on the move, the more or less rapid mobilization of normal or tangential stresses through the normal Kn and tangential Ks rigidities will strongly influence and condition the break mode. It is also recalled that the rupture of one of the two cohesive bonds results in the complete rupture of the cohesive bond. For example, the rupture of the tangential cohesive bond immediately results in the loss of normal cohesion. The effect of each contact parameter on macroscopic tensile behavior will be analyzed individually in this paragraph without excluding the cross-influence of certain parameters. The basic parameters of the parametric study are:

$Kn/Ks=1$ ;  $Kn=7,000,000$  N/m

$Cn/Cs=1$ ;  $Cn=320,000$  N/m

$\mu=0.2$ ;

$\gamma= 20$  kN/m<sup>3</sup>

#### Influence of friction coefficient

The figure 19 shows that the friction coefficient has no effect on the stress-deformation curve. However, this result is only valid in the case of the uni-axial tensile test where the loading path is such that the tangential adhesion erases the effect of the friction coefficient. Indeed, Coulomb's slip condition is inactive at the contact level (by the fact that normal efforts are essentially tensile efforts) as long as the threshold of tangential adhesion is not exceeded.

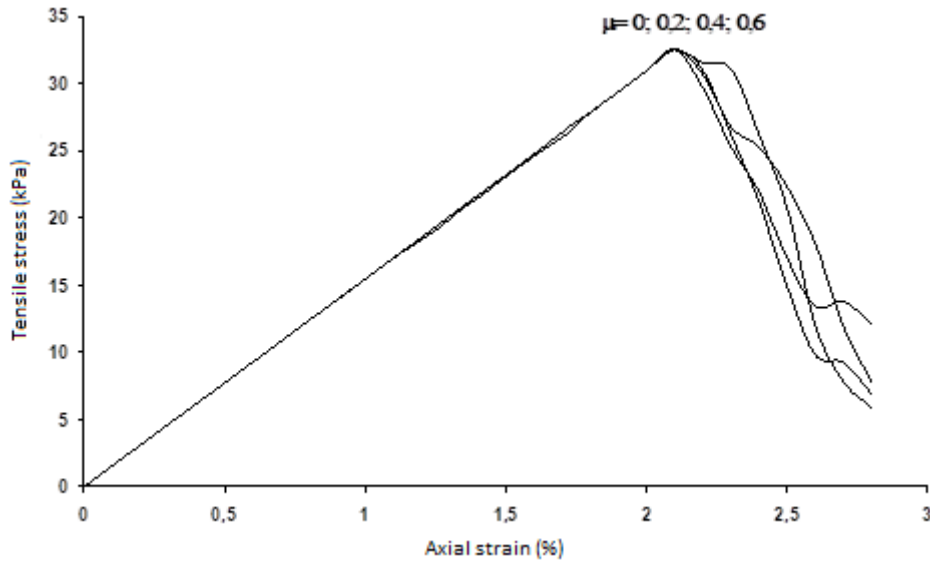


**Figure 19:** Stress-deformation curves during a direct tensile test for different friction coefficients

**Influence of normal and tangential adhesions**

The influence of normal and tangential adhesion on tensile behavior was investigated through a series of numerical simulations based on the basic configuration. The figure 20 shows that the variation in the ratio of adhesions affects tensile strength, but the initial tangent module remains unchanged.

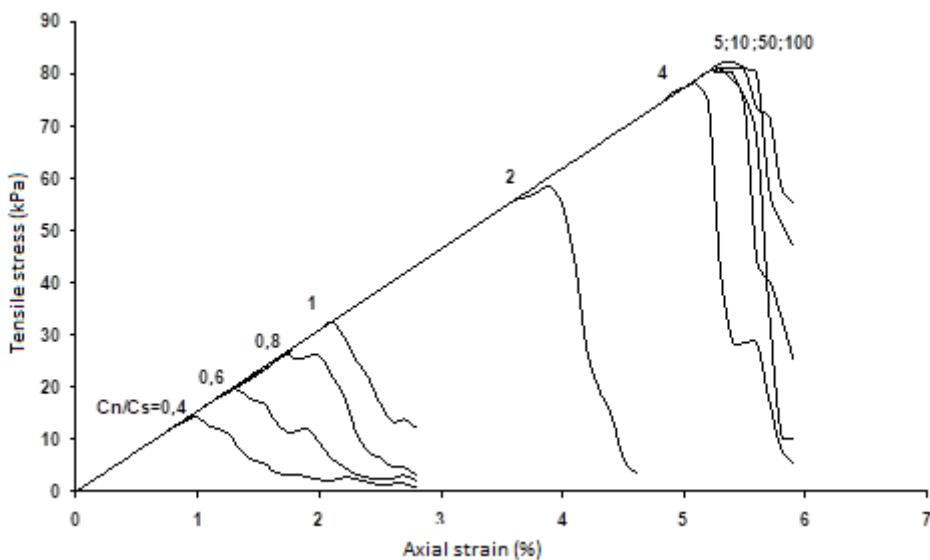


**Figure 20:** Evolution of stress-strain curves for different adhesion ratios

It is noticeable from the figure 21 that tensile strength continues to increase with the ratio of adhesions to a threshold that is reached (for  $k_n/k_s=1$ ) from a  $C_n/C_s$  ratio equal to 5.

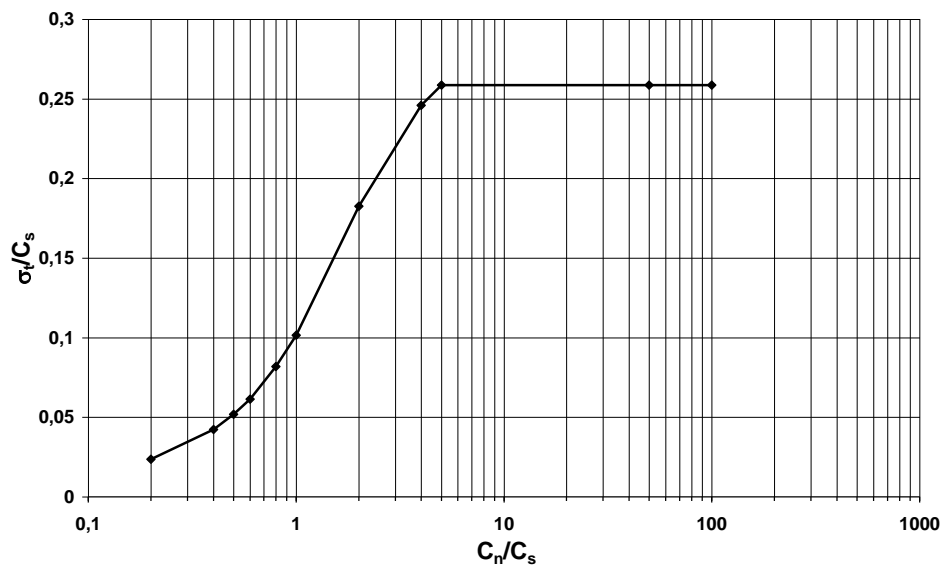


Figure 21: Evolution of dimensionless tensile strength based on adhesion ratio

In order to provide an explanation as to the appearance of the curve on the figure 21, an analysis of the numerically pre-enacted break mode was carried out for various values of the adhesion reports (figure 22).

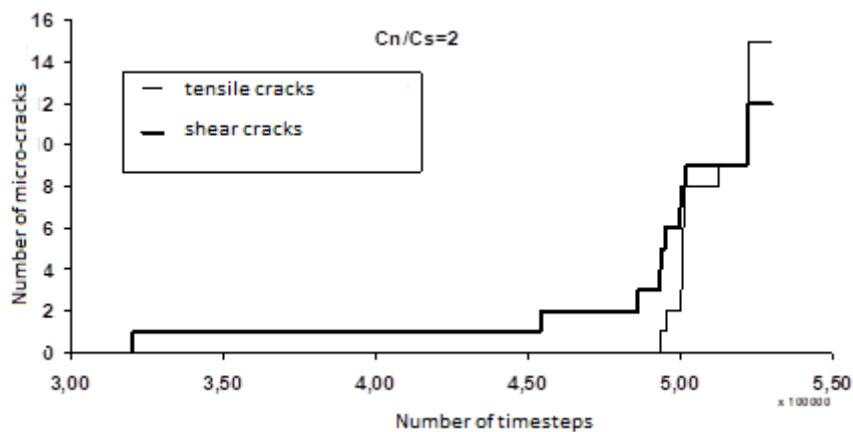


Figure 22: Evolution of micro-cracking during tensile test for  $C_n/C_s=2$

- For  $C_n/C_s$  ratios of 0.2 (a) and 1 (b) (and for  $k_n/K_s=1$ ) micro-cracking is in total normal, i.e. by tensile,
- For a ratio of 2 (c) microcracking is normal and tangential
- for the ratio 10 (d) the microcrackings are purely tangential. Indeed, a relatively large normal adhesion in the face of tangential adherence, leads to the sample being resistant to the sufficiently large leaflet and therefore that only shear break can manifest itself at the level of a set of contacts.

In conclusion, it can be said that for low  $C_n/C_s$  ratios, a low normal adhesion value in relation to tangential adhesion, results in a sample pull break, hence the major influence of the  $C_n$  parameter on the overall tensile behavior of the sample tested. On the other hand, for a ratio of 1, the two ads are equal, so the two different modes of breakage are equiprobable, but the preferred loading paths the tensile threshold. Normal adhesion prevails and influences the value of tensile strength. For  $C_n/C_s$  ratios between 1 and 5, tangential adhesion is likely to play a role, but sollicitation promotes (for  $k_n/k_s=1$ ) normal cracking (by tensile). In this case both types of cracking exist at the same time in the test tube, and therefore the value of the  $C_n/C_s$  ratio still has an influence on the value of tensile strength. Finally for values above 5, normal adhesion is significantly higher than tangential adhesion, all micro-cracks are tangential, which immediately results in the breakdown of the cohesive bond, hence the independence of tensile strength to  $C_n$  for low  $C_s$  values.

**Influence of normal and tangential stiffness**

Several numerical simulations were simulated for different values of the ratio of normal and tangential stiffness. Unlike the adhesion ratio, which has no effect on the initial tangent module, the stiffness ratio has both an effect on the tangent module and the value of tensile strength. The effect of this report on the tangent module is very remarkable.

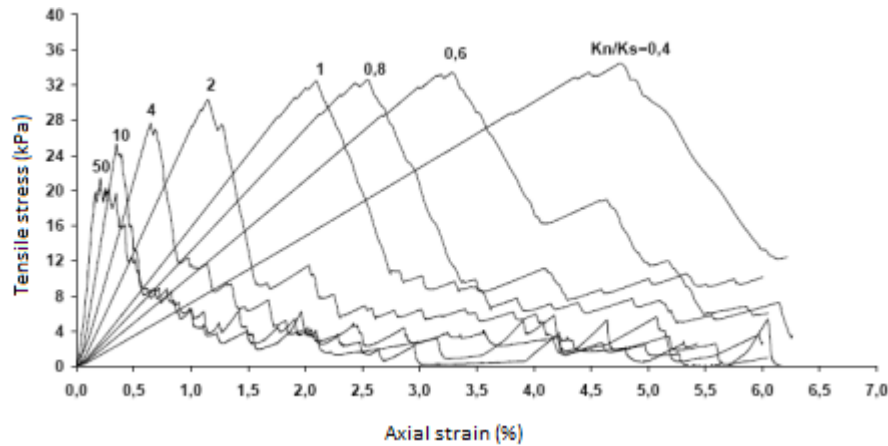


**Figure 23:** Stress – strain curves for different stiffness ratios

The figure 24 shows a close link between the initial tangent module and the stiffness ratio. Indeed it increases with the increase in normal stiffness, since for these results, the ratios were increased to a constant tangential stiffness.

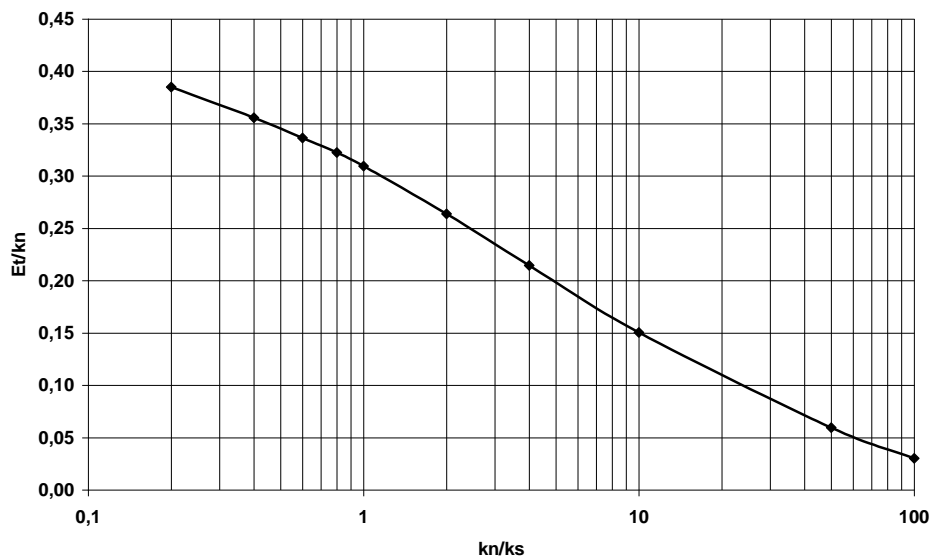


**Figure 24:** The tangent module in tensile based on stiffness ratios

It has been seen previously (for  $K_n/K_s=1$ ) that a  $C_n/C_s=1$  ratio essentially generates tensile micro-cracking. Therefore, for the same kinematics on the move, the increase in  $K_n$  leads to faster reaching the tensile limit of normal adhesion resulting in premature rupture of tensile contacts and a lower sample maximum tensile stress value. Conversely, reducing  $K_n$  can delay the break-up by tensile of the contacts (always effective for  $C_n/C_s=1$ ) and thus mobilize a little more tangential forces, resulting in a slight increase in the maximum pull stress of the sample. If one looks at the cracking mode developed during the test, the figure 25 shows that, regardless of the configuration tested, the mode of rupture of the samples corresponds (for  $C_n/C_s=1$ ) actually to micro-cracking by tensile.

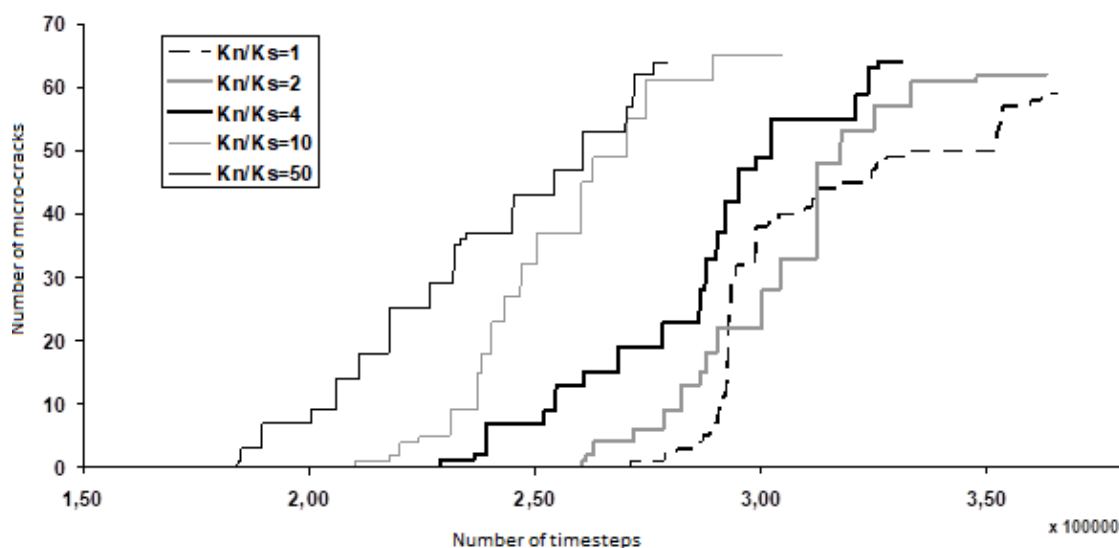


Figure 25: Evolution of micro-cracking by tensile (Cn/Cs-1)

## V. Conclusion

The parametric study of the numerical model was conducted with the aim of quantifying both the effect of micromechanical parameters and numerical parameters for its application for the analysis of the tensile test. As for the "disc" particles used to model the soil, they were a simple discretization of the domain, a minimum number of 2000 particles is sufficient to properly simulate a tensile test. Three criteria were put forward to judge the optimality of the deformation velocity: the mode of rupture, the reproducibility of the test for a given loading threshold, and the maximum amplitude of the average of the unbalanced forces. In addition, a formulation of the progressive application of speed has been proposed to ensure the optimality of convergence. As far as the micro-mechanical parameters of the contact law are concerned, the friction coefficient has no effect on tensile behavior. However, the ratio of normal and tangential adhesions has an effect on tensile strength to a threshold value from which normal adhesion becomes predominant. The ratio of stiffness has a double effect on the tangent module and on tensile strength. Indeed, the tangent module in tensile increases with the value of normal stiffness, while a ratio of adhesions greater than 1 accentuates the mechanisms of micro-cracking by tensile and therefore affects the maximum strength to tensile of Sample.

## References

- [1]. Ammeri, A., Neifar, M., Ibrahim, K. and M Bouassida. Experimental and Numerical Study of the Split Tensile Test on a Silty Soil : Discrete Element Analysis. *International Journal of Engineering Research & Technology (IJERT)*, 5(01), January-2016, pp 929-936.
- [2]. A Ammeri, M Jamei, M Bouassida, O Ple, P Villard, JP Gourc. Numerical study of bending test on compacted clay by discrete element method: tensile strength determination. *International Journal of computer applications in technology* 34 (1),2009, pp 13-22
- [3]. XiaobinDing,Liayang Zhang . A new contact model to improve the simulated ratio of unconfined
- [4]. Compressive strength to tensile strength in bonded particle models.*International Journal of Rock Mechanics & Mining Sciences*69(2014)111–119
- [5]. JinhuiRen ,ZhenghongTian and JingwuBu.Simulating Tensile and Compressive Failure Process of Concrete with a User-defined Bonded-Particle Model. *International Journal of Concrete Structures and Materials*, (2018) 12:56.
- [6]. Tobias Wollborn, Marcelo F. Schwed, UdoFritsching. Direct tensile tests on particulate agglomerates for the determination of tensile strength and interparticle bond forces. *Advanced Powder Technology* 28 (2017) 2177–2185
- [7]. N.E. Yas-ithi, F.Bayram, B.Unver, Y.O zc-elik. Numerical modelling of circular sawing system using discrete element method. *International Journal of Rock Mechanics & Mining Sciences*55(2012)86–96